CFD-based Scouting For The Design of a Multi-fuel Kerosene/Hydrogen Atmospheric Burner

Palanti, Lorenzo ; Mazzei, Lorenzo ; Bianchini, Cosimo ; Link, Sarah; Dave, Kaushal; De Domenico, F.; Gangoli Rao, A.

CFD-BASED SCOUTING FOR THE DESIGN OF A MULTI-FUEL KEROSENE/HYDROGEN ATMOSPHERIC BURNER

Lorenzo Palanti[1], Lorenzo Mazzei[1], Cosimo Bianchini[1],
Sarah Link[2], Kaushal Dave[2], Francesca de Domenico[2] & Arvind Gangoli Rao[2]

[1]Ergon Research SRL, Via Giuseppe Campani 50, 50127, Florence, Italy
[2]Delft University of Technology, Delft 2629 HS, Delft, Netherlands

Abstract

Due to climate change concerns, hydrogen is being considered for future aviation, but its commercial availability is limited, storage is bulky and its combustion with 100% concentration still poses numerous technical challenges. This leads to a certain interest in multi-fuel systems using both hydrogen and kerosene to facilitate the transition without completely redesigning the existing engines. Within the HOPE project, the present study focuses on an innovative multi-fuel combustion concept for aircraft propulsion, considering a laboratory-scale combustor hosted at TU Delft. Such a device, originally fueled with hydrogen and methane, is schematically composed of an axial swirler, four ducts for gaseous fuel injection, a mixing tube and a cylindrical combustion chamber. To avoid flashback, also an axial air injection duct is present that bypasses the swirler and directly reaches the air-fuel mixture in the mixing tube.

In this work, reactive CFD simulations are used to explore different spray injection configurations and assess the impact of kerosene on the flow field, the flame shape and the NO emissions of the modified system. In particular, three different injection positions are studied, featuring injection points on the backplane of the combustion chamber, inside the fuel/air mixing tube or on the axis of the burner. It is found that the most suitable position for kerosene injection is on the axis of the burner, so that the spray is surrounded by the swirling flow and undergoes a rapid mixing with the oxidising stream, limiting the maximum temperature reached by the mixture. Moreover, in this case, the addition of hydrogen leads to reduced NO emissions since it decreases the size of the hot spots generated by the combustion of kerosene.

Keywords: Combustion, Multi-fuel, Hydrogen, Kerosene, CFD.

1. Introduction

Due to growing concerns about climate change, hydrogen has gained significant interest as an alternative option to power the aviation sector in the future. However, neither the fuel nor the engines are widely commercially available nowadays and this situation is not likely to change before the end of this decade [1]. To ease this transition and avoid the complete overhauling of the existing engine technologies as well as airport infrastructures, a multi-fuel system fuelled by both hydrogen and kerosene could represent a promising alternative to the direct adoption of sole hydrogen. The addition of a certain amount of hydrogen has been identified as a valid alternative to enhance kerosene combustion since the 80s [2], but only scattered experimental studies are available in the recent scientific literature [3, 4, 5, 6], most likely due to a relatively small interest in the topic from the aviation sector up to the last couple of years. Even by extending this survey to dual-fuel experiments with other liquid and gaseous fuel mix in constant-volume combustion chambers (i.e. excluding reciprocating engines) only a few works stand out [7, 8].

From a CFD perspective, important efforts have been dedicated so far to the simulation of blends of two gaseous fuels (generally methane and hydrogen) for power generation gas turbines [9] whereas, at the best of the authors' knowledge, only a few researchers tried to address the fundamental problem of the concurrent combustion of liquid kerosene and gaseous hydrogen in aeronautical burners.

In [10] a colourless distributed combustion regime is studied with reactive Reynolds Averaged Navier-Stokes (RANS) simulations: the Discrete Phase Model (DPM) is used to track the spray evolution, whereas the non-premixed model is mentioned to take into account for Turbulence Chemistry Interaction (TCI). On a more fundamental level, Vance et al. [11] carried out the investigation on a 2D premixed laminar flame, using hydrogen, gaseous kerosene and several blends of the two. Due to the laminar regime, no TCI is accounted and the combustion is modelled by transporting all the species contained in the selected reaction mechanism and directly resolving the reaction rate.

If other liquid and gaseous fuels combinations are considered, also other works must be considered. In [12] and in [13], two gas turbine combustion chambers fuelled at the same time by diesel fuel and methane are simulated, with a focus on the pollutant emissions in the first work and on the fuel switching process in the second one. Both rely on the Eddy Dissipation Concept (EDC) model to take into account TCI, whereas the DPM is selected to include liquid atomization and evaporation in the simulation. Concerning turbulence modelling, the RANS approach is used in [12], whereas Large Eddy Simulation (LES) was preferred in [13] because of the improved description of the mixing process and the intrinsic transient phenomenon. Other works [14, 15] deal with the simulation of multi-fuel burners, but none of them actually try to model the concurrent combustion of liquid and gaseous fuel.

The present work is carried out within the Hydrogen Optimized multi-fuel Propulsion system for clean and silEnt aircraft (HOPE) project. In HOPE, the possibility of a multi-fuel aircraft propulsion system is explored, leveraging on the simultaneous use of hydrogen and kerosene. The project seeks to expedite the energy transition in aviation by designing an efficient and fuel-flexible aircraft propulsion system and one of the first steps of this process is the demonstration of multi-fuel combustion on a laboratory scale combustor hosted at TU Delft [16, 17]. In this manuscript, the potential of using a combination of hydrogen and conventional fuels in this burner is addressed from a numerical perspective: CFD is used to simulate how the introduction of kerosene injectors will modify the performance and potentially help to determine the best design to implement in future iterations. Three kerosene injection schemes are studied, each one under three fueling conditions that consist of pure hydrogen, pure kerosene and a mix of the two fuels. Due to the scouting activity, RANS is preferred in this work because of the lower computational effort, even if the need for a more accurate description of the turbulent mixing is highlighted at the end and left for future work. EDC model is selected for TCI as in some of the previous references, because of its ability to deal with the concurrent combustion of two fuels without further modifications. Similarly, DPM is adopted to track the liquid fuel. The work is organised as follows: first, the investigated test rig is introduced along with the three configurations studied and the operating conditions. Then, the numerical setup is discussed, starting from the models employed for turbulence, combustion, liquid fuel and NO formation. In the same section, some new variables to post-process multi-fuel cases are introduced and represent the main novelty of this work. Next, the results achieved for each of one the three injection positions are discussed separately, whereas a cross-comparison is attempted for these three cases fuelled with a mix of hydrogen and kerosene. Finally, some conclusions are drawn along with recommendations for future work.

2. Investigated test rig

The original rig is schematically composed of a combustion chamber, a mixing tube and an axial swirler (see Figure 1), designed with a geometric swirl number of 1.1, based on the approach presented in [18]. All of the oxidizing air is supplied from the bottom: a certain fraction ($\dot{m}_{air,main}$) is fed through four channels, perpendicular to the axis of the burner. Then, it flows through the axial swirler and finally meets the fuel in the mixing tube. The present configuration also incorporates the concept of Axial Air Injection (AAI) [19], where the remaining fraction of the air ($\dot{m}_{air,AAI}$) bypasses the swirler and directly reaches the mixing tube with only an axial velocityy component.

$$AAI = \frac{\dot{m}_{air,AAI}}{(\dot{m}_{air,AAI} + \dot{m}_{air,main})} \tag{1}$$

The amount of air through the AAI can be regulated to prevent the occurrence of flashback. Similarly to the main air, the gaseous fuel is injected through four ducts radially into the swirling flow (marked in red in Figure 1, downstream of the swirler). Thus, the gaseous fuel and combustion air are partially
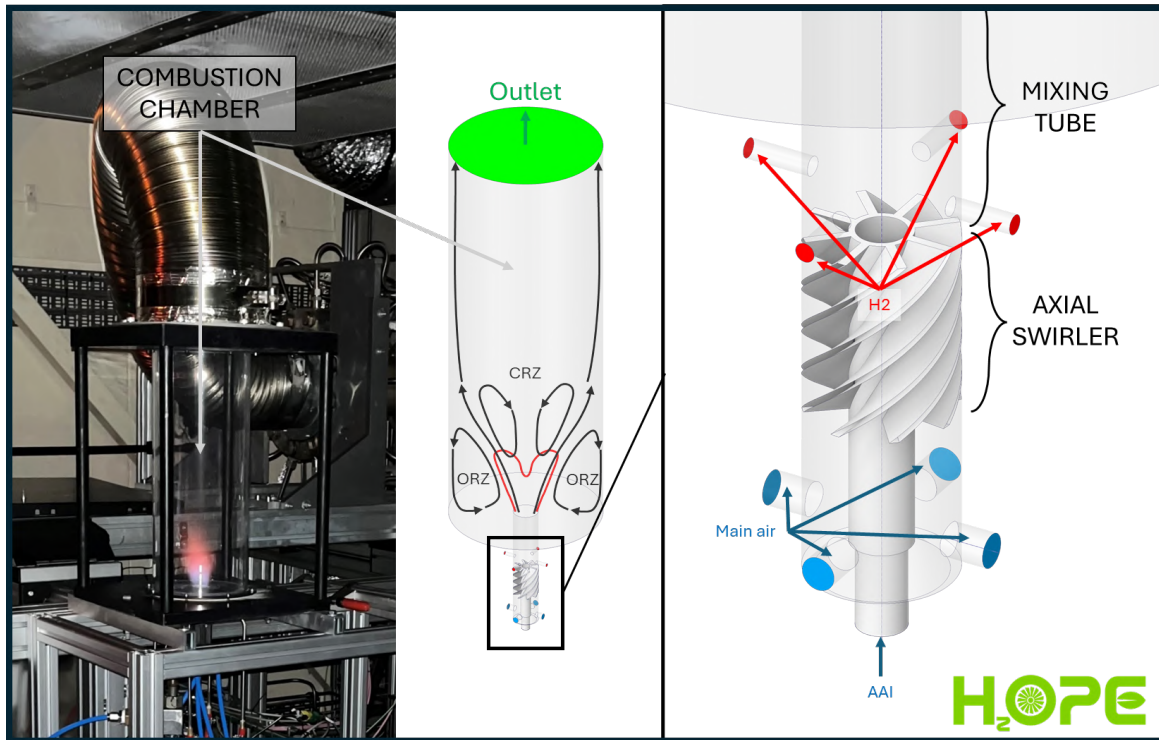
Figure 1 – Picture and sketch of the structure of the rig.

mixed before entering the reaction zone in the combustor. This helps to prevent the formation of stoichiometric hot spots commonly observed in non-premixed configurations. Finally, the combustion chamber is composed of a circular quartz tube allowing optical access and the rig is operated at atmospheric pressure. The experimental setup has already been extensively tested with pure hydrogen, methane, and various blends of the two gases. Additionally, initial tests to demonstrate the feasibility of using the full range of hydrogen and kerosene mixtures in this combustor have been completed using the configuration labelled as INJ-1 in Figure 2.

2.1 Explored configurations

The main purpose of this work is to scout different injection locations for kerosene, introducing only minor modifications to the existing rig. For each one of the three selected locations, three cases are studied including two fuelled with hydrogen or kerosene only, and one with a mix of the two fuels. Such exercise results in the nine configurations shown in Figure 2, which comprise both different kerosene injection locations (columns) as well as fuel compositions (rows). It is worth spending a few words to highlight the main differences between the different kerosene injection locations (columns).

- INJ-1: two atomizers are flush mounted on the backplane of the combustion chamber, far from the mixing tube. Since such configuration requires minimal modifications to the existing hardware, it has already been chosen as a first attempt for the experimental tests.

- INJ-2: to enhance air-fuel mixing, the two atomizers are installed in the mixing tube, facing each other. Kerosene is injected in cross flow and captured by the swirling flow. The formation of a liquid film may occur and it must be addressed properly from a CFD perspective. Note that INJ-1 and INJ-2 are the same if fueling with hydrogen only is considered.

- INJ-3: is introduced as it has a greater resemblance to the architectures of existing burners. The AAI channel is replaced by a duct to supply kerosene to the single injector, installed on the axis of the rig. While the achieved flame shape is more conventional compared to the previous configurations, the possibility of preventing flashback by AAI is lost (but the center of the mixing tube is occupied by the liquid fuel injection system).
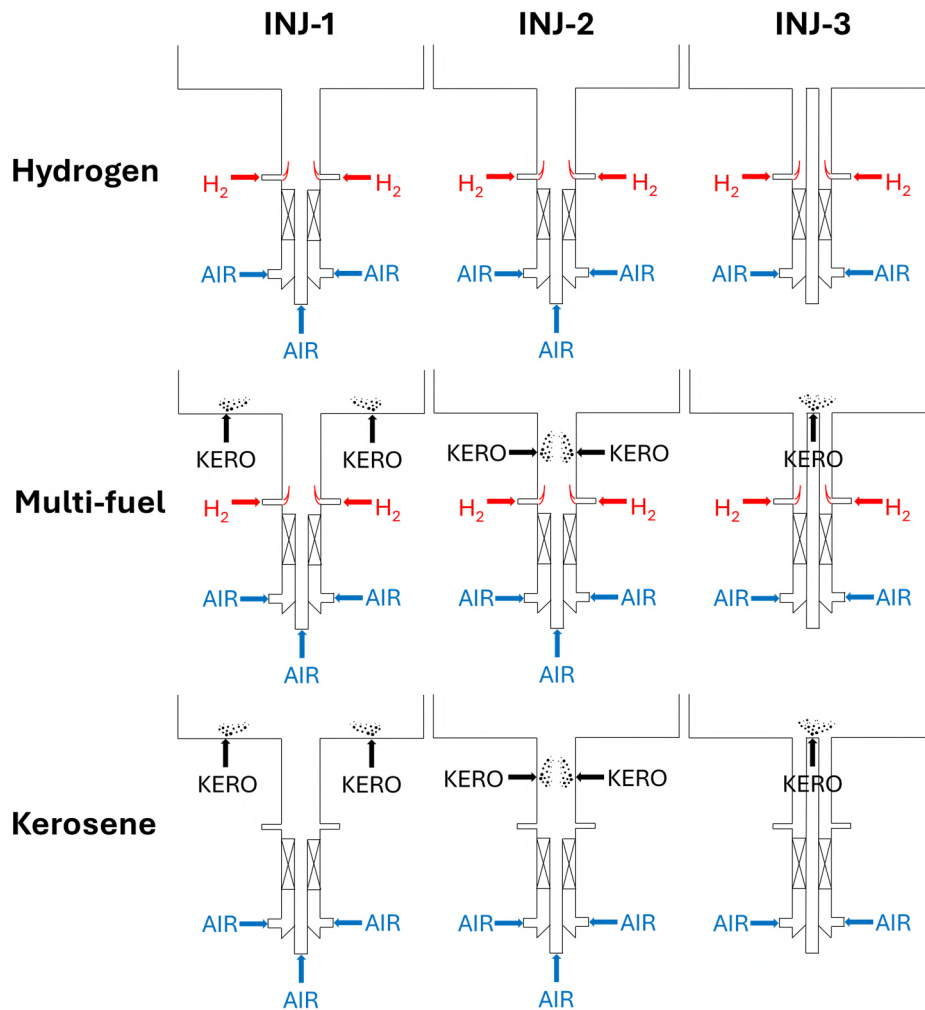
3

Figure 2 – Investigated configurations.

2.2 Operating conditions

The operating conditions are displayed in Table 1. As stated previously, the AAI can be used to prevent flashback when hydrogen alone is employed as fuel. In this work, AAI = 20% is set in INJ-1 and INJ-2 cases, according to the experimental setup, whereas no axial air injection is possible for INJ-3 since the need to install the kerosene injector does not allow to retain this feature.

Case	Kerosene	Multi-fuel	Hydrogen
Thermal power [kW]	11.0	11.0	11.0
Kerosene mass flow rate [g/s]	0.249	0.125	0.0
Kerosene temperature [K]	300	300	-
Hydrogen mass flow rate [g/s]	0.0	0.0458	0.0917
Hydrogen temperature [K]	-	287	287
Total air mass flow rate [g/s]	5.38	5.38	5.38
Air temperature [K]	287	287	287

Table 1 – Simulated operating conditions.

3. Numerical setup

The domain included in the simulation is shown in Figure 3. Periodicity is exploited when possible so that only half of the domain is modelled in INJ-1 and INJ-2 due to the arrangement of the kerosene atomizers (one every 180 degrees). These atomizers are staggered by 45 degrees from the hydrogen
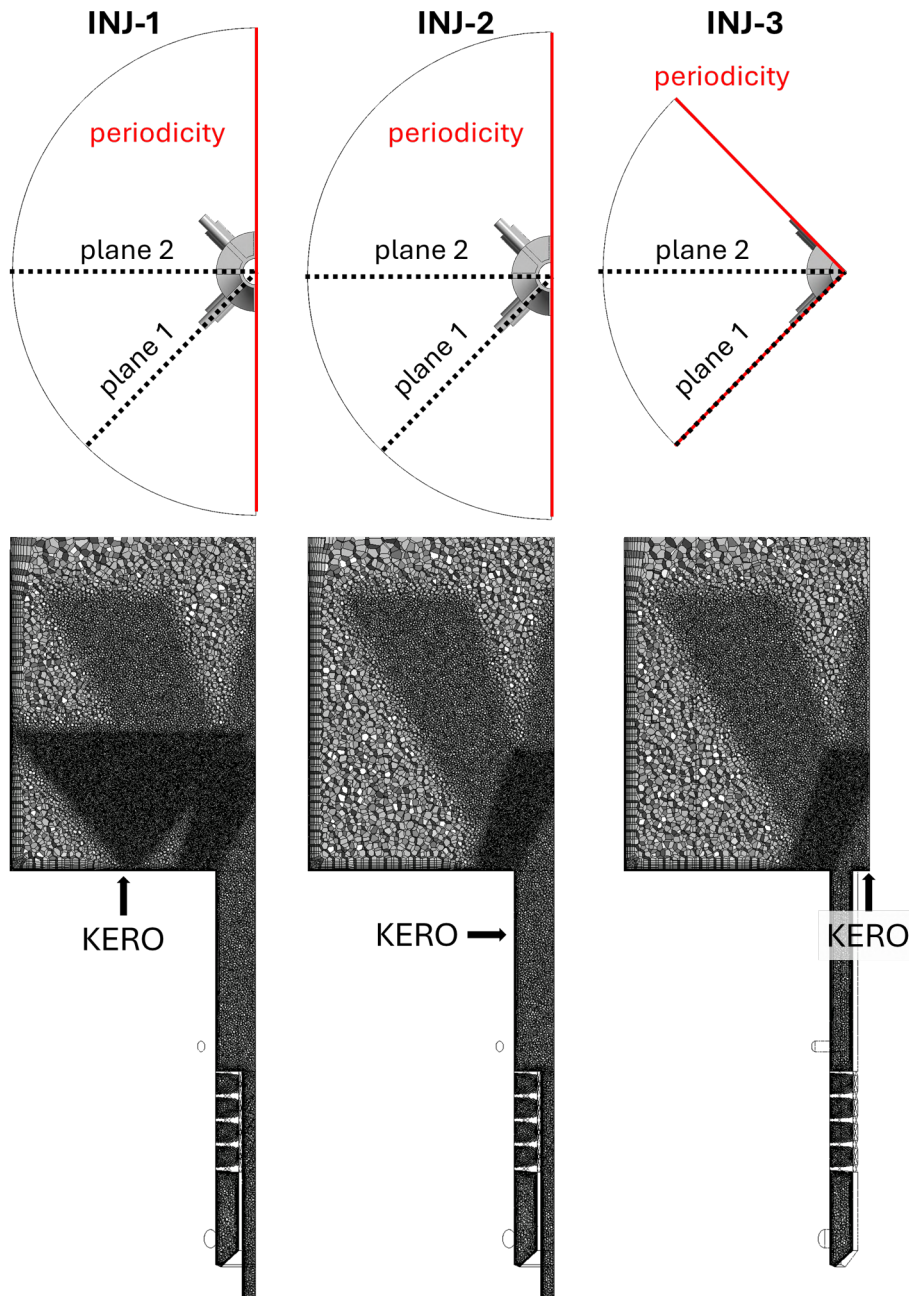
Figure 3 – Numerical domain and mesh of the investigated configurations.

ducts since it could facilitate their installation in the experimental facility. In the same line, in INJ-3 only a quarter of the domain is modelled since the atomizer is placed on the axis and the periodicity of the swirler is exploited. In Figure 3 also the planes used for the post-processing are shown: plane 1 passes through the ducts that supply air and hydrogen to the mixing tube, whereas plane 2 is the one where kerosene is injected in INJ-1 and INJ-2 (as already mentioned, these two planes are staggered by 45 degrees). Moreover, in the same figure also three slices of the computational grids are shown. Similar refinement regions are adopted for the three cases, except for INJ-1 where a greater resolution is needed close to the kerosene injection point. They result in roughly 2.45 M, 1.54 M and 784 k cells for INJ-1, INJ-2 and INJ-3 respectively. Mass flow rate and specified temperature are set for the main air, the AAI and the hydrogen according to Table 1, where the values are reported for the whole domain, not accounting for periodicity. Atmospheric pressure is set at the outlet while all the walls are considered as adiabatic. All the simulations are carried out with the commercial software ANSYS Fluent 2023R2.

3.1 Turbulence and combustion models

The superior accuracy of LES over RANS has been documented several times in literature for the simulation of swirling flows. However, in this work RANS is preferred due to the much lower computational cost and the two-equation model k-ω Shear Stress Transport (SST) [20] is selected as the turbulence model for the simulations. Concerning combustion modelling, the Eddy Dissipation Concept based on the Partially Stirred Reactor (EDC-PaSR) extension [21] is employed. This model belongs to the class of models where the averaged reaction rate is computed and the actual species are transported across the numerical domain [22]. Compared to the models where primitive variables are transported (e.g. flamelet models), it allows the simulation of several streams of fuel and oxidizer with arbitrary compositions, as it is not constrained by the definition of variables such as the mixture fraction [23], that is not trivial when more than one fuel stream is present. Its main limitation consists of the increased computational effort required to solve the transport equations of several species and integrate the chemical reaction rates. Two reaction mechanisms are used in this work: in the cases fuelled only with hydrogen, the San Diego mechanism [24] (9 species and 21 reactions) is chosen whereas the Z77 mechanism by Zetterval et al. [25] is used for multi-fuel and kerosene cases. Z77 is a reduced mechanism for kerosene combustion composed by 30 species and 77 reactions, which exhibits a good agreement against detailed mechanisms by keeping the computational effort relatively low. It is worth noting that a reaction mechanism developed for kerosene combustion is generally capable of effectively modelling hydrogen combustion as well. In particular, as reported in [25], a so-called base sub-mechanism is included in Z77 to describe the combustion of methane that also incorporates a detailed mechanism for hydrogen oxidation.

3.2 Liquid fuel models

The Discrete Phase Model (DPM) is used to track the liquid fuel and to account for its interaction with the continuous phase. Lagrangian particles are directly injected as spherical (primary breakup is modelled) with a specific diameter size distribution depending on the mass flow rate and the estimated pressure drop across the injector. In particular, a Rosin-Rammler distribution is set where the Sauter Mean Diameter (SMD) is calculated using the correlation by Lefebvre [26] for pressure-swirl atomizers and the spread parameter is fixed to q = 3 for all of the cases. In the same line, the injection velocity is adjusted to account for mass flow rate variations. The resulting initial conditions are summarized in Table 2, depending on the number of atomizers installed in each configuration. The drag force

Kerosene mass flow rate [kg/s]	INJ-3 (1 atomizer)			INJ-1 and INJ-2 (2 atomizers)		
	SMD [μm]	q [-]	v [m/s]	SMD [μm]	q [-]	v [m/s]
0.249	12.2	3.0	20.0	20.6	3.0	10.0
0.125	20.6	3.0	10.0	34.6	3.0	5.0

Table 2 – Initial conditions for kerosene injection.

acting on the droplets is modelled with a dynamic drag coefficient based on the Reynolds number [27], the secondary breakup is accounted for through the Stochastic Secondary Droplet (SSD) model [28] and finally the evaporation model described in [29] is employed for mass transfer from the droplet to the continuous phase. In INJ-2, the spray hits the wall of the mixing tube, creates a film of liquid over it, eventually separates at its edge and evaporates in the combustion chamber. This process is accounted for with the Eulerian Wall Film (EWF) model. The continuity and the momentum equations of the film are solved on the surface of the mixing tube so that its local mass, thickness and velocity can be retrieved. Instead, the energy equation of the film is not solved as it is believed to undergo a negligible heat up in the mixing tube, due to the presence of a continuous flow of cold air. The EWF is coupled with the continuous phase through the shear force acting on its surface and also the gravitational force is taken into account. Subsequent film separation and atomization are included as well.

3.3 NO formation model

A consolidated post-processing strategy [30] is used within this work to compute the NO emissions of studied configurations. At first, a converged steady-state RANS simulation is achieved then, all the flow variables are frozen and a specific transport equation for NO is solved through the domain, where its source term is modelled with a dedicated mechanism [31]. In this work, the well-known Zeldovich mechanism is used, so the main driver for NO formation is the local temperature. It is worth mentioning that other pathways are possible, but their impact is usually relevant only when the emissions from the Zeldovich mechanism are extremely low (due to strict control of gas temperature).

3.4 Variables for multi-fuel cases

In multi-fuel cases, it is convenient to define a parameter to describe the ratio between the quantities of the different fuels. Many definitions are possible, either based on mass fractions [3], molar fractions [11], or energy [4, 5, 32, 33], but a standardized parameter has not yet been established in scientific literature. However, a ratio based on the energy (or power) carried by each fuel is by far the most widely used and, in this work, a parameter called global Hydrogen Power Share (HPS_g) is defined as the ratio between the power provided by the hydrogen and the total one from both fuels (Equation 2):

$$HPS_g = \frac{\dot{m}_{H_2} LHV_{H_2}}{\dot{m}_{H_2} LHV_{H_2} + \dot{m}_{kero} LHV_{kero}} \tag{2}$$

Throughout this text, the HPS_g parameter will be used to specify which mix of the two fuels is used so, for the sake of clarity, by $HPS_g = 1.0$ and $HPS_g = 0.0$ the cases with only hydrogen and kerosene are addressed respectively. Finally, it is convenient to define an additional mixing parameter between the two fuels based on their mass, called the global mass fraction of hydrogen within the total fuel (α_g) from now on (Equation 3):

$$\alpha_g = \frac{\dot{m}_{H_2}}{\dot{m}_{H_2} + \dot{m}_{kero}} \tag{3}$$

Thus, $HPS_g = 0.5$ corresponds to roughly $\alpha_g = 0.26$. Along with the HPS_g parameter, it is important to understand whether the combustion is taking place under rich or lean conditions. Thus, the equivalence ratio is introduced and calculated as the ratio between the stoichiometric air-to-fuel ratio and the one of the rig $\phi = AFR_{st}/AFR$. While AFR is simply the ratio between the total mass flow rate of air and fuel (hydrogen and kerosene), AFR_{st} must be defined according to the fuel composition. It can be demonstrated that:

$$AFR_{st} = \alpha_g AFR_{st,H_2} + (1 - \alpha_g) AFR_{st,kero} \tag{4}$$

While all of these quantities are defined at a rig level, also a strategy to post-process the CFD simulations at a local (cell) level must be defined. In particular, it would be interesting to define a quantity that describes the local fuel composition and, similarly to the Bilger mixture fraction [34], does not vary through the combustion process. All the considerations that follow are based on the idea that under unity Lewis number conditions, the local composition in terms of atoms of hydrogen and carbon is directly related to the mixing of the two fuels. Moreover, it is assumed that the oxidizer does not contain carbon. Under these assumptions, a local mass fraction of hydrogen within the total fuel α can be defined prior to combustion as:

$$\alpha = \frac{Y_{H_2}}{Y_{H_2} + Y_{kero}} = \frac{Y_{H_{H_2}} + Y_{C_{H_2}}}{Y_H + Y_C} \tag{5}$$

Where Y_{e_i} is the elemental mass fraction of the element e coming from the fuel species i. It is straightforward that since no carbon is found in the hydrogen, $Y_{C_{H_2}} = 0$. Thus, the elemental mass fraction of hydrogen coming from gaseous hydrogen $Y_{H_{H_2}}$ can be recast as $Y_H - Y_{H_{kero}}$, where Y_H is the elemental mass fraction of hydrogen that can easily be computed from CFD results. Assuming a certain fuel surrogate for the kerosene (for instance $C_{12}H_{23}$ in the present work), the elemental mass fraction of hydrogen from kerosene $Y_{H_{kero}}$ is directly linked to its composition in terms of atoms and the local α can be expressed as:

$$\alpha = \frac{Y_H - \frac{a_{H,kero} W_H}{a_{C,kero} W_C} Y_C}{Y_H + Y_C} \tag{6}$$

Where $a_{H,kero}$ and $a_{C,kero}$ are the number of hydrogen and carbon atoms in kerosene (fixed by the selected surrogate) whereas W_C and W_H are the molar weight of carbon and hydrogen respectively. Note that $(a_{H,kero}W_H)/(a_{C,kero}W_C)$ is a constant. Equation 6 is rather interesting as it is not affected by the reactive process and can be calculated anywhere in the numerical domain of a reactive simulation. It not only allows the description of the mixing process taking place between the two fuels but it can also be used to properly define the local equivalence ratio (equations are omitted here for the sake of brevity) and thus understand if lean or rich combustion is taking place, regardless of the fuel composition. Finally, also a local Hydrogen Power Share HPS can be computed thanks to α:

$$HPS = \frac{\alpha LHV_{H_2}}{\alpha LHV_{H_2} + (1-\alpha)LHV_{kero}} \tag{7}$$

It can be used as an alternative indication of the mixing between the two fuels or to understand which fuel is carrying most of the energy to a certain area of the burner.

4. Results

At the beginning of this section, the main results are shown independently for each one of the studied configurations, to provide a rough idea of the flow and temperature fields originated by the different fuel injections. Then, a cross-comparison between the three injection strategies is shown, to illustrate the main differences in terms of mixing and how the variables introduced in the previous section can help to post-process a multi-fuel configuration. Finally, NO emissions are discussed. For the sake of brevity, only reactive simulations are shown here.

4.1 Configuration INJ-1

INJ-1 corresponds to the configuration that is currently under investigation at TU Delft. The flow field resulting from this injection strategy is reported in Figure 4 in terms of velocity magnitude. As anticipated, the contours are plotted on two planes (described in Figure 3) for the three values of HPS_g, namely $HPS_g = 0.0$ (kerosene only), $HPS_g = 0.5$ (multi-fuel) and $HPS_g = 1.0$ (hydrogen only). In $HPS_g = 0.0$, a classic swirled flame structure is achieved despite the presence of the AAI (that
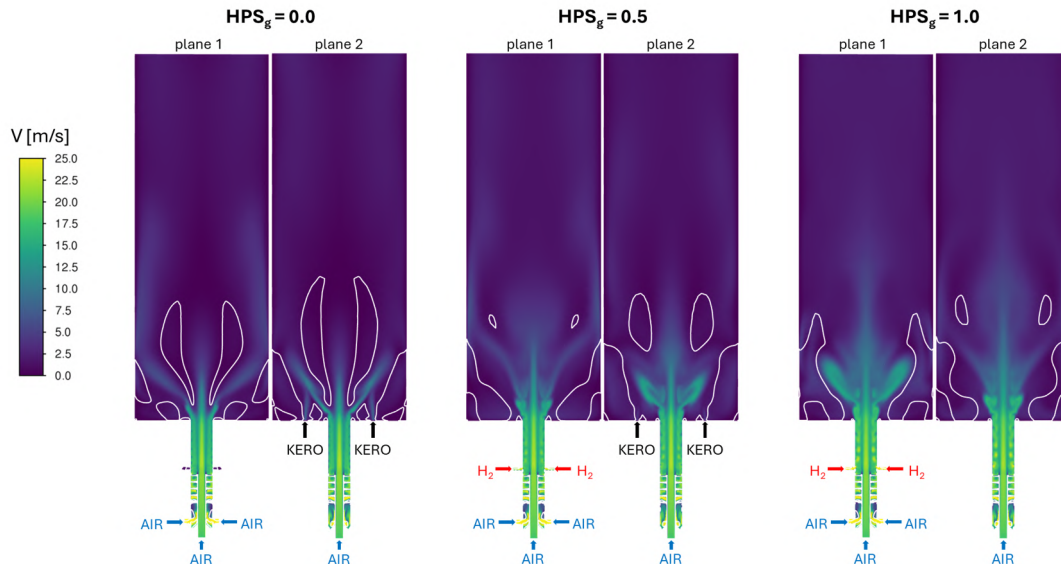

Figure 4 – Velocity fields for INJ-1 under the three studied hydrogen power shares. White iso-lines at local zero axial velocity.

usually disrupts the flow recirculation within the swirling flow). A toroidal Central Recirculation Zone (CRZ), pierced by the AAI flow on the axis, and an Outer Recirculation Zone (ORZ) can be found, highlighted by the white iso-lines at zero axial velocity (see also Figure 1). In addition, the spray injection is visible on plane 2 and affects the shape of the swirling flow, locally reducing its opening angle. When the hydrogen is injected (and consistently the kero is reduced to achieve $HPS_g = 0.5$),

the swirling flow is altered significantly. The addition of hydrogen creates two effects in the mixing tube: the acceleration of the air-hydrogen mixture (thanks to its low density) and the reduction in the swirl component due to its radial momentum. Overall, this disrupts the swirling flow and reduces the opening angle. The CRZ is almost suppressed by the reduced angular momentum of the swirling flow which merges together with the AAI. The ORZ is preserved and occupies a larger fraction of the domain. Moreover, the high-speed spots associated with spray injection almost disappear due to the halved mass flow rate, the reduced injection velocity and the limited momentum exchange with the continuous phase. At $HPS_g = 1.0$, the effects are further exacerbated: the increased axial velocity due to the mass addition in the mixing tube along with the action of the radial injection leads to a marked reduction in the tangential component of velocity. This suppresses the vortex breakdown and the swirl stabilization of the flame, which appears more similar to a jet flame configuration.

The associated temperature fields are reported in Fig 5 together with white-iso lines at heat release rate $10^7 [W/m^3]$ to identify the flame front. In INJ-1, relatively cold regions can be found in corre-
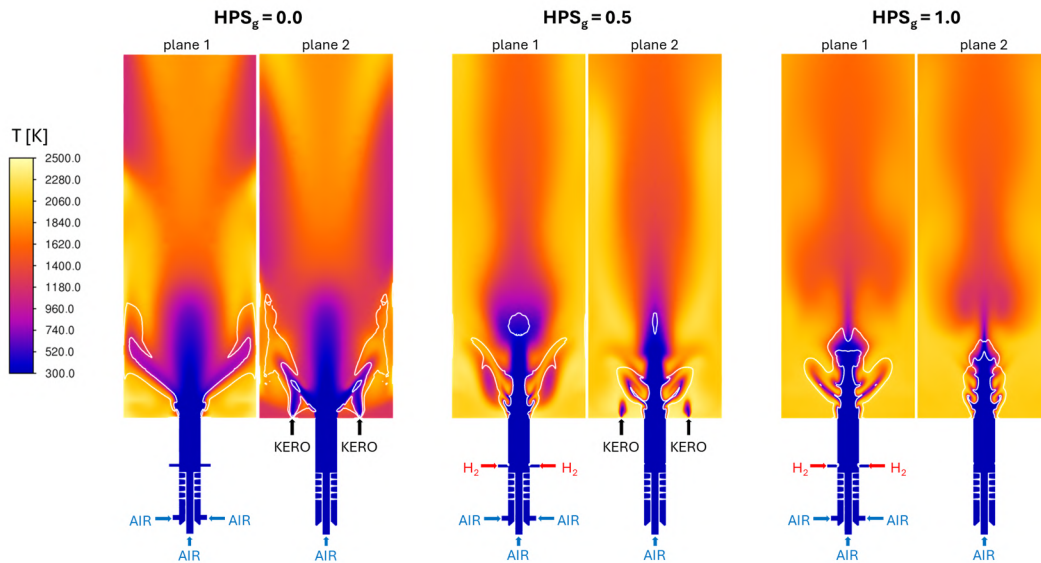

Figure 5 – Temperature fields for INJ-1 under the three studied hydrogen power shares. White iso-lines at heat release rate = $10^7 [W/m^3]$.

spondence with the swirling flow, the central AAI and close to the fuel injection due to the local heat sink generated by the liquid evaporation. The flame is stabilized by the presence of the ORZ and the CRZ, which provide two regions of low-velocity and high-temperature gases. By increasing the fraction of hydrogen in the configurations $HPS_g = 0.5$ and $HPS_g = 1.0$, the ORZ becomes larger and hotter than in $HPS_g = 0.0$. The flame moves closer to the axis of the burner and stabilizes in the shear layer between the ORZ and the central jet (composed by the swirling flow and the AAI, since the CRZ is suppressed). Some cold streaks branch off from the central cold flow, protruding towards larger radial coordinates and generating peculiar curved shapes. These can be attributed to the four streaks of hydrogen, issued by the four hydrogen injection ducts inside in the swirled flow: they leave the mixing tube before being fully premixed and assume a sort of spiral shape in three dimensions, which is then cut by the two planes here considered. Considering the RANS approach on which the simulations are based, it is reasonable to expect that the turbulent mixing is underestimated and that the presence of these unusual shapes would be mitigated by using higher fidelity approaches such as LES.

4.2 Configuration INJ-2

The results from INJ-2 are condensed in Figure 6. The supposed advantage of this configuration would be to avoid the injection of fuel directly in the hot environment of the combustion chamber such as INJ-1, allowing the liquid fuel to further break up and evaporate before reaching the combustion chamber. However, since the airflow is rather cold in all of these cases, evaporation is very little and
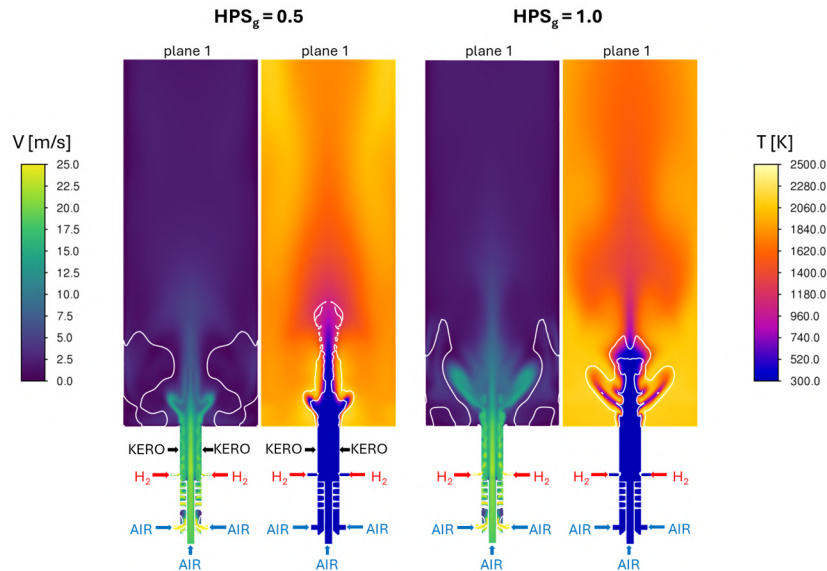
Figure 6 – Velocity and temperature fields for INJ-2 for $HPS_g = 0.5$ and 1.0. White iso-lines at local zero axial velocity and heat release rate $= 10^7 [W/m^3]$.

due to the relatively low velocity of the gas inside the mixing tube, the spray crosses it and reaches the opposite wall forming a film over it. Under these peculiar conditions, it was not possible to achieve a solution for $HPS_g = 0.0$, since the force of gravity pulling the film downwards inside the swirler is larger than the aerodynamic one (exercised by the mixture) that should drag it upwards into the combustion chamber. For this reason, INJ-2 is not feasible under the present operating conditions making it pointless to discuss it in greater detail. However, velocity and temperature results for $HPS_g = 0.5$ and $HPS_g = 1.0$ are reported in Figure 6, on plane 1 only for the sake of brevity. It is worth recalling that $HPS_g = 1.0$ is not discussed again as it is the same as INJ-1, since the two configurations differ only for the kerosene injection strategy. Compared to INJ-1 at $HPS_g = 0.5$, here also the spray injection forces the reduction of the tangential component of the velocity inside the mixing tube. Thus, as noted in the previous configuration, the CRZ is suppressed completely and a sort of long jet flame is generated. Due to the low velocity of the gaseous flow in the mixing tube and the absence of an actual prefilmer to enhance atomization, the droplets that separate from the mixing tube edge are rather large and undergo very slow evaporation. As a result, part of the kerosene does not burn before leaving the domain, which makes this solution not acceptable for the purpose of reducing pollutant emissions.

4.3 Configuration INJ-3

In the end, the results for INJ-3 are shown. Before deep diving into the description of the achieved results, it is worth mentioning that a significant modification is made here by removing the AAI duct and placing the kerosene injection on the axis of the burner. As a consequence, the possibility to prevent flashback is lost, even if the liquid fuel injection system is providing some blockage that should hinder its occurrence. Moreover, from a mechanical perspective, it would be very difficult to install a commercial pressure atomizer on the current structure due to the limited size of the mixing tube, but addressing these considerations is postponed to a further phase of the work.

As already done for INJ-1, the resulting flow field is shown in Figure 7 for three levels of HPS_g and on the two planes shown in Figure 3. Compared to previous cases, the velocity inside the mixing tube is higher due to the same mass flow rate passing through a smaller duct. This results in an increased pressure drop across the injector, which must be compensated for by the laboratory infrastructure. Similarly to other laboratory burners, all investigated HPS_g configurations exhibit a large Central Recirculation Zone (CRZ), highlighted by the white iso-lines. In contrast, the size of the Outer Recirculation Zone (ORZ) is limited by the wide opening angle of the swirling jet. In $HPS_g = 0.0$ and $HPS_g = 0.5$ the kerosene injection is clearly visible on the axis of the burner but does not significantly affect the swirling flow, which looks very similar in the three cases. Higher velocities are found in the
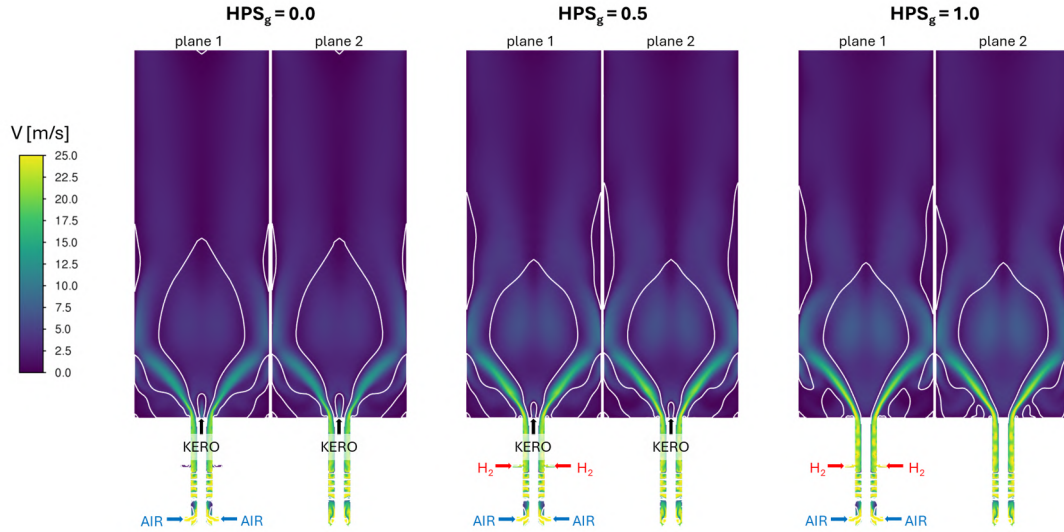
Figure 7 – Velocity field for INJ-3 under the three studied hydrogen power shares. White iso-lines at local zero axial velocity.

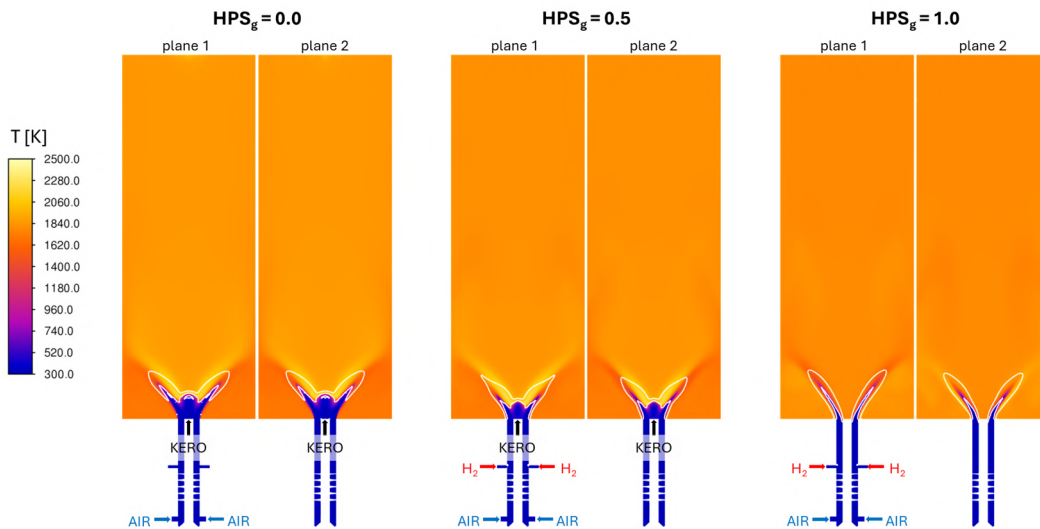swirling flow by adding hydrogen in both $HPS_g = 0.5$ and 1.0 cases.

Figure 8 – Temperature field for INJ-3 case under the three studied hydrogen power shares. White iso-lines at heat release rate = $10^7 [W/m^3]$.

The temperature field (Figure 8) is rather uniform compared to the previous configurations, due to the enhanced mixing induced by the higher flow velocity. At $HPS_g = 0.0$, the evaporation of the spray cools down the area close to the injection. The flame is established in the CRZ, which leads to high temperature areas where the kerosene vapor meets the airflow from the swirling flow. The addition of hydrogen ($HPS_g = 0.5$) slightly reduces the flame length, as it is particularly clear from the shorter length of the cold jet generated by the mixing tube. If only hydrogen is injected, a very good pre-mixing is obtained and the flame does not show any significant hot spot. Despite that, the flame is attached to the central kerosene injector, potentially causing flashback and mechanical integrity issues. This suggests the necessity of refining the work by considering a more realistic shape of the injector nozzle and higher fidelity approaches such as LES.

4.4 Cross-comparison of multi-fuel cases

While many papers have been published concerning hydrogen or kerosene combustion in the scientific literature, at the best of the authors' knowledge this is one of the first regarding a multi-fuel

configuration. Therefore, it is interesting to highlight some of the differences between the studied injection strategies when fuelled with both fuels. In Figure 9, the equivalence ratio is shown. First
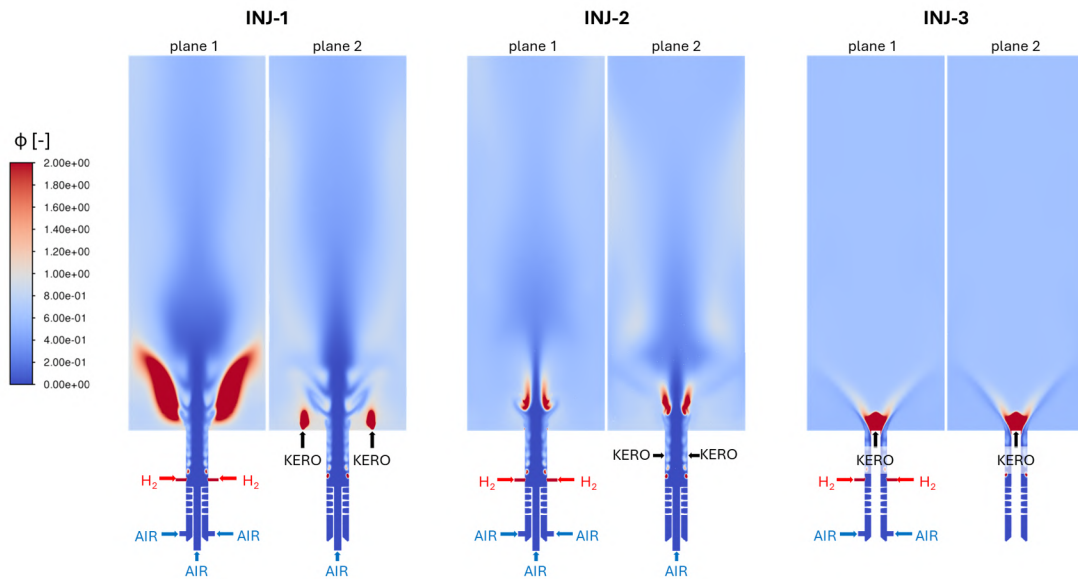

Figure 9 – Equivalence ratio field for the three studied injection strategies at $HPS_g = 0.5$.

of all, only in INJ-3 a very good mixing can be pointed out at the end of the domain, whereas in the other cases, a larger variability of the equivalence ratio can be found. In particular in INJ-1 and INJ-2, the core of the flow is leaner due to the AAI, whereas it appears slightly richer close to the lateral walls of the combustion chamber. In INJ-1, the rich area associated with spray injection propagates deep into the combustion chamber, which can cause potential issues associated with NO and soot emissions. A similar behaviour is found in INJ-2 but in a much more limited region. In INJ-3 a rich area is found only where the spray is injected, but it rapidly mixes with a leaner mixture coming from the swirler. Finally, it is important to note that the ORZ is close to stoichiometric conditions in INJ-1, which can potentially lead to a high-temperature zone with a long residence time (an ideal condition for high NO emissions).

While the equivalence ratio can be used to evaluate the mixing between fuel and air, it is also important to understand how the two fuels mix among them. To do so, in Figure 10 the contours of the hydrogen mass fraction within fuel (α) defined in the previous section are shown. It is important to recall the global value for the rig is $\alpha_g = 0.26$. As for the equivalence ratio, the configuration which exhibits a better mixing is INJ-3. Here the ORZ is a bit more filled by hydrogen products, whereas in the CRZ most of the kerosene combustion products are found. Instead, in INJ-1 and INJ-3 the mixing between the two fuels is not completed even at the end of the rig. Finally, it is worth showing the same contour but scaled by the energy carried by the two fuels (Figure 11). Similar conclusions can be drawn but thanks to the different scale used, it is even easier to determine in which zone one of the two fuels is more relevant than the other. Once more, better mixing is achieved in INJ-3, whereas larger regions of hydrogen/kerosene predominance are found in the other two configurations. It is worth remembering however that such results are affected by the steady-state RANS approach, which typically underestimates turbulent mixing compared to LES.

4.5 NO emissions

In Figure 12 the NO emissions are shown for the investigated configurations. They are displayed in parts per million and scaled to an oxygen content of 15%. As expected from the previous results, INJ-3 leads to the lowest emissions as it does not display significant hot spots. In all of the three HPS_g a very good mixing is achieved and a maximum of 50 ppm is predicted for the pure kerosene case. Also considering that it is injected and atomized directly over the flame, lower NO emissions were not expected for this case. However, the addition of hydrogen allows for a reduction of the emissions as hydrogen likely burns in a fully premixed regime. At $HPS_g = 1.0$, around 8 ppm are
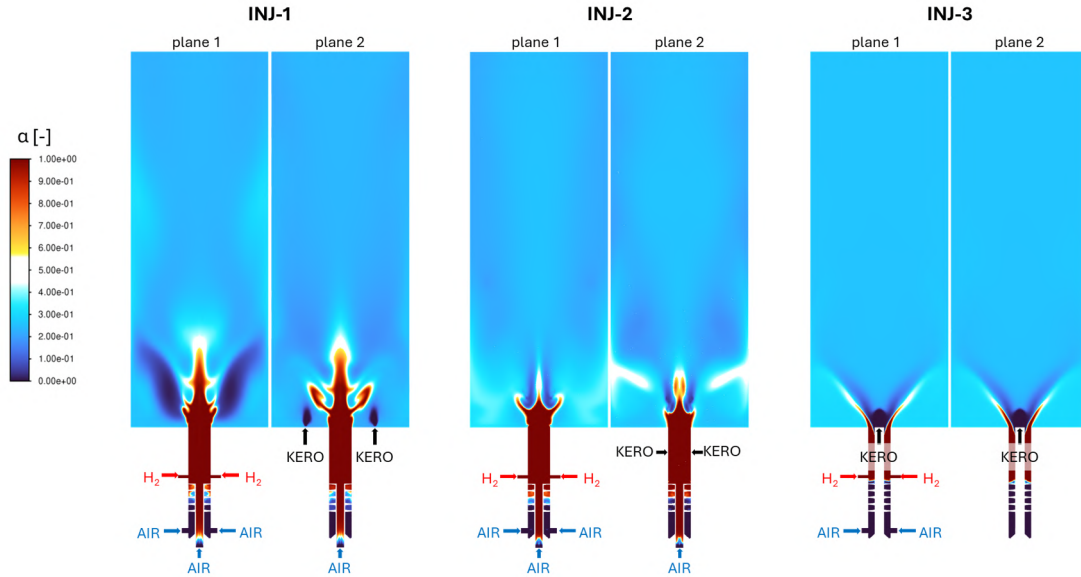
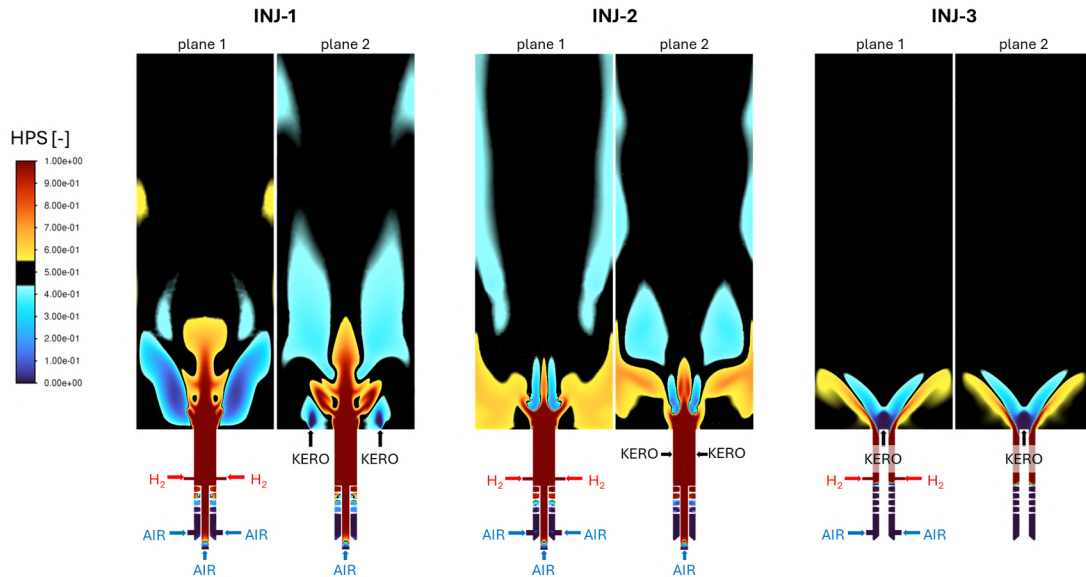Figure 10 – α field for the three studied injection strategies at $HPS_g = 0.5$.

Figure 11 – Local HPS field for the three studied injection strategies at $HPS_g = 0.5$.

estimated, which is consistent with a perfectly premixed lean flame fueled by hydrogen. Extremely large emissions are found for the other two cases, mostly due to the hot spots located in the ORZ. Moreover, due to the suppression of the CRZ, the ORZ is very large and the residence time is supposedly longer, leading to very high emissions despite the lean conditions. It is worth noting how in INJ-1 using two fuels ($HPS_g = 0.5$) leads to increased emissions compared to $HPS_g = 0.0$ and $HPS_g = 1.0$. This might be due to the poor mixing between the two fuels shown in Figure 11, which creates two flames that are almost separated in the domain, further increasing the volume where stoichiometric equivalence ratio can be found as well as the associated high-temperature spots. It is important to note that very high emissions are predicted, which have not been empirically observed by TUD in their experiments (not yet published). As previously mentioned, this discrepancy is partly due to the use of the RANS approach. Selected for its lower computational cost, RANS sacrifices some accuracy, often underestimating turbulent mixing. This can lead to inaccuracies in predicting the mixing inside the mixing tube and, consequently, the flame shape. Additionally, all walls were considered adiabatic, but heat losses could significantly lower the temperature in the ORZ, potentially reducing NO emissions. Despite the poor quantitative estimation, the relative variations in
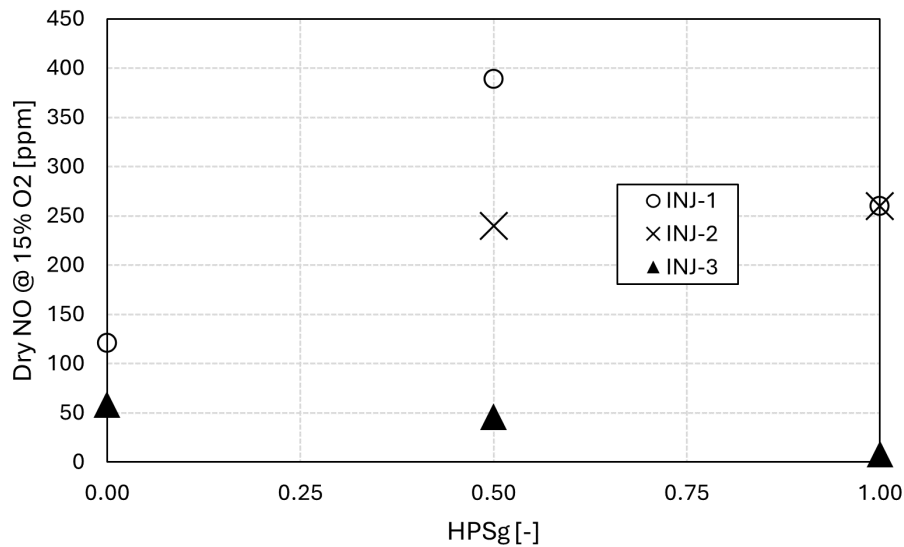
Figure 12 – NO emissions of the studied configurations.

emissions under different operating conditions (e.g., fuel composition) are usually more accurate and can provide useful insights. For instance, in INJ-3 at $HPS_g = 0.5$, there is a reduction in emissions compared to $HPS_g = 0.0$, a trend not observed in INJ-1. While the predicted emission values may be overestimated or underestimated, it is reasonable to believe that such variations would be confirmed in reality, as they are likely due to the differing flow fields that should occur similarly in experiments.

5. Conclusions

The work was carried out as part of the HOPE project, which aims to develop a novel aircraft propulsion system that can be fueled alternatively or simultaneously by hydrogen and kerosene. The goal is to facilitate the hydrogen transition in aviation without necessitating a complete redesign of current engines and airport infrastructures. Computational Fluid Dynamics (CFD) was used to explore three different kerosene injection strategies, to implement them in an existing laboratory test rig at TUD, which is currently fueled only by hydrogen. The three injection strategies differ in the number and position of the atomizers, as well as in the method of mixing hydrogen and air. For each configuration, three operating conditions were studied: one fueled by hydrogen, one by kerosene, and one with an equal share of the two in terms of supplied power. RANS simulations were used to compare the proposed configurations in terms of flow field, temperature, mixing performance, and emissions. Additionally, some novel parameters to quantify the mixing between the two fuels are introduced and used for the first time in this paper. In the INJ-1 configuration, the ORZ is large and hot, leading to high NOx emissions. The local hydrogen power share indicates poor mixing between the two fuels, which may also impact emissions. It was also found that the INJ-2 configuration is not feasible under the current operating conditions. So far, the INJ-3 configuration appears the most promising in terms of reducing pollutant emissions. The idea is that by moving the kerosene injection on the axis and improving its mixing with hydrogen, a more uniform temperature field can be achieved, thereby keeping NOx emissions relatively low. However, the resistance to flashback, the mechanical integrity of the central kerosene injector, and the feasibility of manufacturing it still need to be verified. In the next phases, the work will focus on exploring additional configurations, using also a different combustion model (FGM) to verify the $HPS_g = 0.0$ and 1.0 conditions, as well as employing Large Eddy Simulation (LES) to enhance the prediction of turbulent mixing in the most promising configurations.

6. Funding

7. Contact Author Email Address

All correspondence regarding this paper should be addressed to: lorenzo.mazzei@ergonresearch.it.

8. Copyright Statement

References

[1] Efstathios-Al. Tingas and Alex M. K. P. Taylor. *Hydrogen: Where it Can Be Used, How Much is Needed, What it May Cost*, page 3–64. Green Energy and Technology. Springer International Publishing, Cham, 2023.

[2] Hiroyuki Hiroyasu, Masataka Arai, Toshikazu Kadota, and Jiro Yoso. An Experimental Study on Kerosene-Hydrogen Hybrid Combustion in a Gas Turbine Combustor. *Bulletin of JSME*, 23(184):1655–1662, 1980.

[3] G Juste. Hydrogen injection as additional fuel in gas turbine combustor. Evaluation of effects. *International Journal of Hydrogen Energy*, 31(14):2112–2121, November 2006.

[4] J.P. Frenillot, G. Cabot, M. Cazalens, B. Renou, and M.A. Boukhalfa. Impact of H2 addition on flame stability and pollutant emissions for an atmospheric kerosene/air swirled flame of laboratory scaled gas turbine. *International Journal of Hydrogen Energy*, 34(9):3930–3944, May 2009.

[5] Joseph Burguburu, Gilles Cabot, Bruno Renou, Abdelkrim M. Boukhalfa, and Michel Cazalens. Effects of H2 enrichment on flame stability and pollutant emissions for a kerosene/air swirled flame with an aeronautical fuel injector. *Proceedings of the Combustion Institute*, 33(2):2927–2935, 2011.

[6] Luigi Miniero, Khushboo Pandey, Gianluigi De Falco, Andrea D'Anna, and Nicolas Noiray. Soot-free and low-NO combustion of Jet A-1 in a lean azimuthal flame (LEAF) combustor with hydrogen injection. *Proceedings of the Combustion Institute*, 39(4):4309–4318, 2023.

[7] Ogbonnaya Agwu, Jon Runyon, Burak Goktepe, Cheng Tung Chong, Jo-Han Ng, Anthony Giles, and Agustin Valera-Medina. Visualisation and performance evaluation of biodiesel/methane co-combustion in a swirl-stabilised gas turbine combustor. *Fuel*, 277:118172, October 2020.

[8] Ogbonnaya Agwu and Agustin Valera-Medina. Diesel/syngas co-combustion in a swirl-stabilised gas turbine combustor. *International Journal of Thermofluids*, 3–4:100026, May 2020.

[9] S. Taamallah, K. Vogiatzaki, F.M. Alzahrani, E.M.A. Mokheimer, M.A. Habib, and A.F. Ghoniem. Fuel flexibility, stability and emissions in premixed hydrogen-rich gas turbine combustion: Technology, fundamentals, and numerical simulations. *Applied Energy*, 154:1020–1047, September 2015.

[10] Hüsamettin Alperen Alabaş and Bilge Albayrak Çeper. Effect of the hydrogen/kerosene blend on the combustion characteristics and pollutant emissions in a mini jet engine under CDC conditions. *International Journal of Hydrogen Energy*, 52:1275–1287, January 2024.

[11] Faizan Habib Vance, Hendrik Nicolai, and Christian Hasse. A numerical investigation into the stabilization of hydrogen enriched n-dodecane premixed flames. *International Journal of Hydrogen Energy*, 56:611–620, February 2024.

[12] Serhiy Serbin, Badri Diasamidze, Viktor Gorbov, and Jerzy Kowalski. Investigations of the emission characteristics of a dual-fuel gas turbine combustion chamber operating simultaneously on liquid and gaseous fuels. *Polish Maritime Research*, 28(2):85–95, June 2021.

[13] Chuanlong Hu, Fuquan Deng, Xiao Liu, Shilin Yan, Jinghe Lu, Chengwen Sun, and Hongtao Zheng. Large eddy simulation of combustion characteristics during dual fuel switching process in gas turbine combustor. *International Journal of Heat and Fluid Flow*, 106:109329, April 2024.

---

[14] Hongtao Zheng, Gang Pan, Xi Chen, and Xiaoming Hu. Effect of dual fuel nozzle structures on combustion flow field in crgt combustor. *Mathematical Problems in Engineering*, 2013:1–11, 2013.

[15] Gang Pan, Hongtao Zheng, Chunliang Zhou, and Zhijia Song. Numerical research on dual fuel combustor combustion performance. In *Volume 6A: Energy*, page V06AT07A015, San Diego, California, USA, November 2013. American Society of Mechanical Engineers.

[16] Sarah Link, Kaushal Dave, Georg Eitelberg, Arvind Gangoli Rao, and Francesca de Domenico. THE INFLUENCE OF THE CONFINEMENT RATIO ON THE PRECESSING VORTEX CORE DYNAMICS IN A COUNTER-ROTATING DUAL SWIRLER. 2023.

[17] Gioele Ferrante, Lennard Doodeman, Arvind Gangoli Rao, and Ivan Langella. LES OF HYDROGEN-ENRICHED METHANE FLAMES IN A LEAN-BURN COMBUSTOR WITH AXIAL AIR INJECTION. 2023.

[18] N. Syred and J.M. Beér. Combustion in swirling flows: A review. *Combustion and Flame*, 23(2):143–201, 1974.

[19] Thoralf Reichel. *Flashback Prevention in Lean-Premixed Hydrogen Combustion*. PhD thesis, 07 2017.

[20] Florian R Menter. Improved two-equation k-omega turbulence models for aerodynamic flows. Technical report, 1992.

[21] Michał T. Lewandowski, Alessandro Parente, and Jacek Pozorski. Generalised eddy dissipation concept for mild combustion regime at low local reynolds and damköhler numbers. part 1: Model framework development. *Fuel*, 278:117743, 2020.

[22] Thierry Poinsot and D. Veynante. *Theoretical and Numerical Combustion*. Edwards, Philadelphia, 2nd ed edition, 2005.

[23] R.W. Bilger. The structure of turbulent nonpremixed flames. *Symposium (International) on Combustion*, 22(1):475–488, January 1989.

[24] Priyank Saxena and Forman A Williams. Testing a small detailed chemical-kinetic mechanism for the combustion of hydrogen and carbon monoxide. *Combustion and Flame*, 145(1-2):316–323, 2006.

[25] N. Zettervall, C. Fureby, and E.J.K. Nilsson. A reduced chemical kinetic reaction mechanism for kerosene-air combustion. *Fuel*, 269:117446, June 2020.

[26] A Lefebvre. *Atomization and Sprays*. Combustion (Hemisphere Publishing Corporation). Taylor Francis, 1988.

[27] Alex B Liu, Daniel Mather, and Rolf D Reitz. Modeling the effects of drop drag and breakup on fuel sprays. *SAE Transactions*, pages 83–95, 1993.

[28] SV Apte, Mikhael Gorokhovski, and Parviz Moin. Les of atomizing spray with stochastic modeling of secondary breakup. *International Journal of Multiphase Flow*, 29(9):1503–1522, 2003.

[29] Sergei S Sazhin. Advanced models of fuel droplet heating and evaporation. *Progress in energy and combustion science*, 32(2):162–214, 2006.

[30] Daniele Pampaloni, Pier Carlo Nassini, Simone Paccati, Lorenzo Palanti, Antonio Andreini, Bruno Facchini, Matteo Cerutti, and Giovanni Riccio. Numerical predictions of pollutant emissions of novel natural gas low nox burners for heavy duty gas turbine. In *2018 Joint Propulsion Conference*, Cincinnati, Ohio, July 2018. American Institute of Aeronautics and Astronautics.

[31] Ronald K. Hanson and Siamak Salimian. *Survey of Rate Constants in the N/H/O System*, page 361–421. Springer New York, New York, NY, 1984.

[32] Ismail Hakki Hakkı Akçay, Habib Gürbüz, Hüsameddin Akçay, and Mustafa Aldemir. An investigation of euro diesel-hydrogen dual-fuel combustion at different speeds in a small turbojet engine. *Aircraft Engineering and Aerospace Technology*, 93(4):701–710, July 2021.

[33] Habib Gürbüz, Hüsameddin Akçay, Mustafa Aldemir, İsmail Hakkı Akçay, and Ümit Topalcı. The effect of euro diesel-hydrogen dual fuel combustion on performance and environmental-economic indicators in a small uav turbojet engine. *Fuel*, 306:121735, December 2021.

[34] R.W. Bilger, S.H. Stårner, and R.J. Kee. On reduced mechanisms for methaneair combustion in non-premixed flames. *Combustion and Flame*, 80(2):135–149, 1990.